

A Numerical Rocks Physics Approach to Model Wave Propagation in Hydrocarbon Reservoirs

III Workshop en Modelado, Migración e Inversión
Sísmica, Junio 20-23, 2017

Juan E. Santos,

Instituto del Gas y del Petróleo (IGPUBA), Universidad de Buenos Aires
(UBA), Argentina, Department of Mathematics, Purdue University, West
Lafayette, Indiana, USA, and Universidad Nacional de La Plata (UNLP),
Argentina.

In collaboration with P. M. Gauzellino (UNLP), G. B. Savioli (UBA), A.
Sanchez Camus (UNLP) and R. Martinez Corredor, (UNLP).

June 15, 2017

Seismic waves in fluid-saturated poroelastic materials. I

- Fast compressional or shear waves travelling through a fluid-saturated porous material (a **Biot medium**) containing heterogeneities on the order of centimeters (mesoscopic scale) suffer attenuation and dispersion observed in seismic data.
- The **mesoscopic loss** effect occurs because different regions of the medium may undergo different strains and fluid pressures.
- This in turn induces **fluid flow and Biot slow waves** causing energy losses and velocity dispersion due to energy transfer between wave modes.

Seismic waves in fluid-saturated poroelastic materials. II

- Since **extremely fine meshes** are needed to represent these type of mesoscopic-scale heterogeneities, numerical simulations are very expensive or not feasible.
- Alternative: In the context of **Numerical Rock Physics**, perform compressibility and shear time-harmonic experiments to determine a long-wave equivalent viscoelastic medium to a highly heterogeneous Biot medium.
- This viscoelastic medium has in the average the same attenuation and velocity dispersion than the highly heterogeneous Biot medium.
- Each experiment is associated with a **Boundary Value Problem (BVP)** that is solved using the **Finite Element Method (FEM)**.

Biot's equations in the diffusive range of frequencies.

Frequency-domain stress-strain relations in a Biot medium

$$\begin{aligned}\tau_{kl}(\mathbf{u}) &= 2G \epsilon_{kl}(\mathbf{u}^s) + \delta_{kl} \left(\lambda_u \nabla \cdot \mathbf{u}^s + B \nabla \cdot \mathbf{u}^f \right), \\ p_f(\mathbf{u}) &= -B \nabla \cdot \mathbf{u}^s - M \nabla \cdot \mathbf{u}^f,\end{aligned}$$

$$\mathbf{u} = (\mathbf{u}^s, \mathbf{u}^f), \quad \mathbf{u}^s = (u_1^s, u_3^s), \quad \mathbf{u}^f = (u_1^f, u_3^f).$$

Biot's equations in the diffusive range:

$$\begin{aligned}\nabla \cdot \boldsymbol{\tau}(\mathbf{u}) &= 0, \\ i\omega \mu \kappa^{-1} \mathbf{u}^f + \nabla p_f(\mathbf{u}) &= 0,\end{aligned}$$

μ : fluid viscosity, κ : frame permeability.

The complex P-wave modulus of the long-wave equivalent viscoelastic medium. I

Introduction

A viscoelastic
medium long-wave
equivalent to a
Biot's medium. I

Variational
formulation. The
FEM

Application to the
cases of patchy
gas-brine
saturation and
highly
heterogeneous
frames

Fractured Biot
media

A VTI long-wave
equivalent to a
fractured Biot's
medium. I

The Macroscale.
Wave propagation

Biots' s equations are be solved in the 2-D case on square sample $\Omega = (0, L)^2$ with boundary $\Gamma = \Gamma^L \cup \Gamma^B \cup \Gamma^R \cup \Gamma^T$ in the (x_1, x_3) -plane. The domain Ω is a representative sample of our fluid saturated poroelastic material.

$$\begin{aligned}\Gamma^L &= \{(x_1, x_3) \in \Gamma : x_1 = 0\}, & \Gamma^R &= \{(x_1, x_3) \in \Gamma : x_1 = L\}, \\ \Gamma^B &= \{(x_1, x_3) \in \Gamma : x_3 = 0\}, & \Gamma^T &= \{(x_1, x_3) \in \Gamma : x_3 = L\}.\end{aligned}$$

For determining the complex plane wave modulus, we solve Biots' s equations with the boundary conditions

$$\begin{aligned}\tau(\mathbf{u})\nu \cdot \nu &= -\Delta P, & (x_1, x_3) &\in \Gamma^T, \\ \tau(\mathbf{u})\nu \cdot \chi &= 0, & (x_1, x_3) &\in \Gamma, \\ \mathbf{u}^s \cdot \nu &= 0, & (x_1, x_3) &\in \Gamma^L \cup \Gamma^R \cup \Gamma^B, \\ \mathbf{u}^f \cdot \nu &= 0, & (x_1, x_3) &\in \Gamma.\end{aligned}$$

The complex P-wave modulus of the long-wave equivalent viscoelastic medium. II

The *equivalent* undrained complex plane-wave modulus $\overline{E}_u(\omega)$ is determined by the relation

$$\frac{\Delta V(\omega)}{V} = -\frac{\Delta P}{\overline{E}_u(\omega)},$$

valid for a viscoelastic homogeneous medium in the quasi-static case. V : original volume of the sample. Then to approximate $\Delta V(\omega)$ use

$$\Delta V(\omega) \approx Lu_3^{s,T}(\omega),$$

$u_3^{s,T}(\omega)$: average vertical solid displacements $u_3^s(x_1, L, \omega)$ on Γ^T .

The complex shear modulus of the long-wave equivalent viscoelastic medium. I

Solve Biots' s equations with the boundary conditions

$$-\tau(\mathbf{u})\nu = \mathbf{g}, \quad (x_1, x_3) \in \Gamma^T \cup \Gamma^L \cup \Gamma^R,$$

$$\mathbf{u}^s = 0, \quad (x, y) \in \Gamma^B,$$

$$\mathbf{u}^f \cdot \nu = 0, \quad (x, y) \in \Gamma,$$

$$\mathbf{g} = \begin{cases} (0, \Delta G), & (x_1, x_3) \in \Gamma^L, \\ (0, -\Delta G), & (x_1, x_3) \in \Gamma^R, \\ (-\Delta G, 0), & (x_1, x_3) \in \Gamma^T. \end{cases}$$

The change in shape of the rock sample allows to recover its *equivalent* complex shear modulus $\overline{G}_u(\omega)$ using the relation

$$\text{tg}(\theta(\omega)) = \frac{\Delta T}{\overline{G}_u(\omega)},$$

$\theta(\omega)$: departure angle from the original positions of the lateral boundaries

The complex shear modulus of the long-wave equivalent viscoelastic medium. II

Introduction

A viscoelastic
medium long-wave
equivalent to a
Biot's medium. I

Variational
formulation. The
FEM

Application to the
cases of patchy
gas-brine
saturation and
highly
heterogeneous
frames

Fractured Biot
media

A VTI long-wave
equivalent to a
fractured Biot's
medium. I

The Macroscale.
Wave propagation

To find an approximation to $\text{tg}(\theta(\omega))$, compute the average horizontal displacement $u_1^{s,T}(\omega)$ of the horizontal displacements $u_1^s(x_1, L, \omega)$ at the top boundary Γ^T . Then use

$$\text{tg}(\theta(\omega)) \approx u_1^{s,T}(\omega)/L,$$

that allows to determine the shear modulus $\overline{G}_u(\omega)$

The complex P-wave and shear velocities are

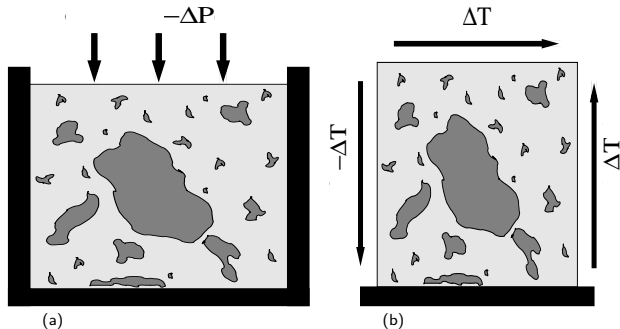
$$v_{sc}(\omega) = \sqrt{\frac{\overline{G}_u(\omega)}{\overline{\rho}}}, \quad v_{pc}(\omega) = \sqrt{\frac{\overline{E}_u(\omega)}{\overline{\rho}}},$$

The compressional phase velocities $v_p(\omega)$, $v_s(\omega)$ and quality factor $Q_p(\omega)$, $Q_s(\omega)$ are

$$v_p(\omega) = \left[\operatorname{Re} \left(\frac{1}{v_{pc}(\omega)} \right) \right]^{-1}, \quad \frac{1}{Q_p(\omega)} = \frac{\operatorname{Im}(v_{pc}(\omega)^2)}{\operatorname{Re}(v_{pc}(\omega)^2)},$$

$$v_s(\omega) = \left[\operatorname{Re} \left(\frac{1}{v_{sc}(\omega)} \right) \right]^{-1}, \quad \frac{1}{Q_s(\omega)} = \frac{\operatorname{Im}(v_{sc}(\omega)^2)}{\operatorname{Re}(v_{sc}(\omega)^2)}.$$

Schematic representation of the experiments to determine the complex P-wave and shear modulus



Figures (a) show how to determine $\bar{E}_u(\omega)$, (b) show how to determine $\bar{G}_u(\omega)$.

$$H^{1,P}(\Omega) = \{\mathbf{v} \in [H^1(\Omega)]^2 : \mathbf{v} \cdot \nu = 0 \text{ on } \Gamma^L \cup \Gamma^R \cup \Gamma^B\},$$

$$H_{0,B}^{1,T}(\Omega) = \{\mathbf{v} \in [H^1(\Omega)]^2 : \mathbf{v} = 0 \text{ on } \Gamma^B\},$$

$$H_0(\text{div}, \Omega) = \{\mathbf{v} \in [L^2(\Omega)]^2 : \nabla \cdot \mathbf{v} \in L^2(\Omega), \mathbf{v} \cdot \nu = 0 \text{ on } \Gamma\}.$$

$$\mathcal{V}^{(P)} = [H^{1,P}(\Omega)]^2 \times H_0(\text{div}; \Omega), \mathcal{V}^{(T)} = [H_{0,B}^{1,T}(\Omega)]^2 \times H_0(\text{div}; \Omega).$$

Let

$$\begin{aligned} \Lambda(\mathbf{u}, \mathbf{v}) = & i\omega \left(\mu \kappa^{-1} \mathbf{u}^f, \mathbf{v}^f \right) + \sum_{l,m} (\tau_{lm}(\mathbf{u}), \varepsilon_{lm}(\mathbf{v}^s)) \\ & - \left(p_f(\mathbf{u}), \nabla \cdot \mathbf{v}^f \right) \end{aligned}$$

To determine $\bar{E}_u(\omega)$: find $u^{(P)} = (u^{(s,P)}, u^{(f,P)}) \in \mathcal{V}^{(P)}$ such that

$$\Lambda(\mathbf{u}^{(P)}, \mathbf{v}) = - \langle \Delta P, \mathbf{v}^s \cdot \nu \rangle_{\Gamma T}, \quad \forall \quad \mathbf{v} = (\mathbf{v}^s, \mathbf{v}^f) \in \mathcal{V}^{(P)}.$$

To determine $\bar{G}_u(\omega)$: find $\mathbf{u}^{(T)} = (\mathbf{u}^{(s,T)}, \mathbf{u}^{(f,T)}) \in \mathcal{V}^{(T)}$ such that

$$\Lambda(\mathbf{u}^{(T)}, \mathbf{v}) = - \langle \mathbf{g}, \mathbf{v}^s \rangle_{\Gamma \setminus \Gamma^B}, \quad \forall \quad \mathbf{v} = (\mathbf{v}^s, \mathbf{v}^f) \in \mathcal{V}^{(S)}.$$

$$\mathcal{N}^{h,P} = \{\mathbf{v} : \mathbf{v}|_{R^j} \in [P_{1,1}(R^j)]^2, \mathbf{v} \cdot \nu = 0 \text{ on } \Gamma^L \cup \Gamma^R \cup \Gamma^B\}$$

$$\mathcal{N}_{0,B}^{h,T} = \{\mathbf{v} : \mathbf{v}|_{R^j} \in [P_{1,1}(R^j)]^2, \mathbf{v} = 0 \text{ on } \Gamma^B\} \cap [C^0(\bar{\Omega})]^2.$$

$$\mathcal{V}_0^h = \{\mathbf{v} : \mathbf{v}|_{R^j} \in P_{1,0} \times P_{0,1}, \mathbf{v} \cdot \nu = 0 \text{ on } \Gamma\}.$$

$$\mathcal{V}^{(h,P)} = \mathcal{N}^{h,P} \times \mathcal{V}_0^h, \quad \mathcal{V}^{(h,T)} = \mathcal{N}_{0,B}^{h,T} \times \mathcal{V}_0^h.$$

$P_{s,t}$: polyn. of degree not greater than s in x_1 and not greater than t in x_3 .

The FE procedures to determine $\bar{E}_u(\omega)$ and $\bar{G}_u(\omega)$:

$$\Lambda(\mathbf{u}^{(h,P)}, \mathbf{v}) = - \langle \Delta P, \mathbf{v}^s \cdot \nu \rangle_{\Gamma^T}, \quad \forall \mathbf{v} = (\mathbf{v}^s, \mathbf{v}^f) \in \mathcal{V}^{(h,P)},$$

$$\Lambda(\mathbf{u}^{(h,T)}, \mathbf{v}) = - \langle \mathbf{g}, \mathbf{v}^s \rangle_{\Gamma \setminus \Gamma^B}, \quad \forall \mathbf{v} = (\mathbf{v}^s, \mathbf{v}^f) \in \mathcal{V}^{(h,T)}.$$

The mesh size h , it has to be small enough so that diffusion process associated with the fluid pressure equilibration is accurately resolved.

The diffusion length is given by the relation length

$$L_d = \sqrt{\frac{2\pi\kappa K_f}{\mu\omega}},$$

We take h so that the minimum diffusion length is discretized with at least 3 mesh points at the highest frequency, which is sufficient to represent a (smooth) diffusion-type process.

Besides, the size of the rock sample is not arbitrary: it has to be big enough to constitute a representative part of the Biot medium but, at the same time, it has to be much smaller than the wavelengths associated with each frequency.

Application to patchy gas-brine saturation

Patchy gas-brine saturation arises in hydrocarbon reservoirs, where regions of non-uniform patchy saturation occur at gas-brine contacts. Patchy-saturation patterns produce very important **mesoscopic loss effects at the seismic band of frequencies**, as was first shown by J. E. White (GPY, 1975).

To study these effects, consider porous samples with spatially variable gas-brine distribution in the form of irregular patches fully saturated with gas and zones fully saturated with brine. The domain Ω is a square of side length 50 cm, and a 75×75 mesh uniform is used.

The frequency is varied from 0 to 500 Hz and the solid matrix is sandstone 1 with properties given in Table 1. The fluids properties are given in Table 2.

Table: Physical properties of the solid materials

	Sandstone 1	Sandstone 2	Shale
K_s	37 GPa	37 GPa	25 GPa
ρ_s	2650 kg/m ³	2650 kg/m ³	2650 kg/m ³
ϕ	0.3	0.2	0.3
K_m	4.8 GPa	12.1 GPa	3.3 GPa
μ_m	5.7 GPa	14.4 GPa	1.2 GPa
κ	10 ⁻¹² m ²	0.23 × 10 ⁻¹² m ²	1.5 × 10 ⁻¹⁷ m ²

Introduction

A viscoelastic medium long-wave equivalent to a Biots medium. I

Variational formulation. The FEM

Application to the cases of patchy gas-brine saturation and highly heterogeneous frames

Fractured Biot media

A VTI long-wave equivalent to a fractured Biots medium. I

The Macroscale. Wave propagation

Properties of the fluids used in the experiments.

Table: Physical properties of the fluids

	Brine	Gas
K_f	2.25 GPa	0.012 GPa
ρ_f	1040 kg/m ³	78 kg/m ³
η	0.003 Pa · s	0.00015 Pa · s

Patchy gas-brine distribution for two different correlation lengths

Juan E. Santos,

Introduction

A viscoelastic medium long-wave equivalent to a Biot's medium. I

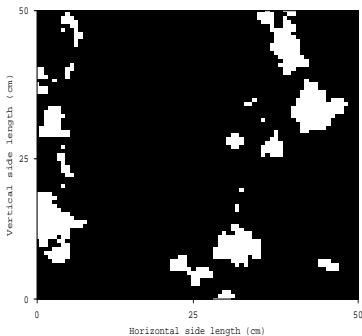
Variational formulation. The FEM

Application to the cases of patchy gas-brine saturation and highly heterogeneous frames

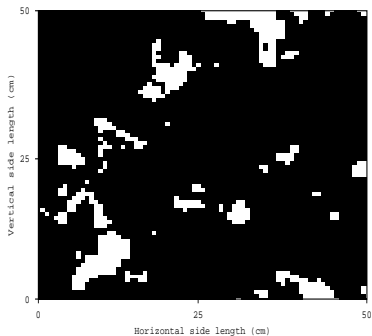
Fractured Biot media

A VTI long-wave equivalent to a fractured Biot's medium. I

The Macroscale. Wave propagation



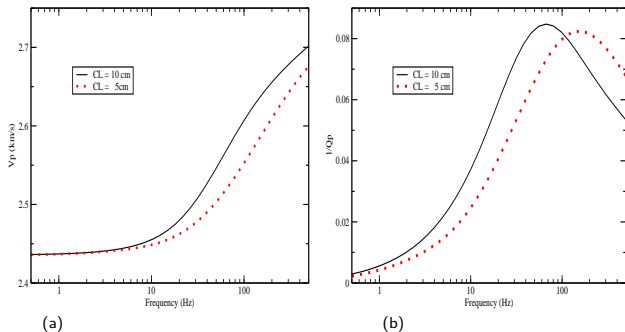
(a)



(b)

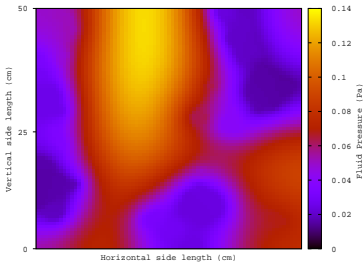
(a): correlation length 10 cm (b): correlation lengths 5 cm.

Compressional phase velocity and inverse quality factors for two different correlation lengths CL



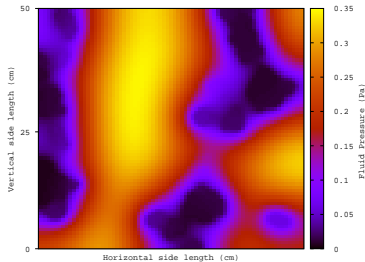
(a): Compressional phase velocity (b): Inverse quality factors. Notice the attenuation peak moving to higher frequencies for the shorter CL.

Pressure distribution (Pa) at two different frequencies.



(a)

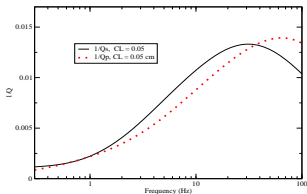
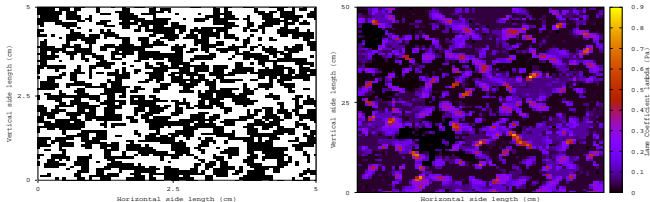
(a): 10 Hz



(b)

(b): 60 Hz.

Gradient of pressures can be seen at the gas-water interfaces, stronger at 65 Hz than at 10 Hz. This Figure illustrates the mesoscopic loss mechanism.



Top left: Fractal shale-sandstone 2 distribution. Black zones correspond to pure shale and white ones to pure sandstone 2. Shale percentage is 50 %. Top right: Absolute fluid pressure distribution (Pa) at 30 Hz. Bottom: Inverse quality factors Q_S and Q_P . Q_S of about 75 between 20 and 40 Hz, Q_P about 70 at 65 Hz. **Conclusion:** wave induced fluid flow (mesoscopic loss) is observed when shear and compressional waves propagate through Biot media with highly heterogeneous solid frames.

- **Fractures** are common in the earth's crust due to different factors, for instance, tectonic stresses and natural or artificial hydraulic fracturing caused by a pressurized fluid.
- **Seismic wave propagation** through **fractures and cracks** is an important subject in exploration and production geophysics, earthquake seismology and mining.
- **Fractures** constitute the sources of earthquakes, and hydrocarbon and geothermal reservoirs are mainly composed of **fractured rocks** .

- Modeling fractures requires a suitable interface model. Nakagawa and Schoenberg (JASA (2007)) presented a set of **boundary conditions (B.C.)** to represent fluid-solid interaction within a fracture and the effect of its permeability on seismic wave scattering.
- At a fracture, these **B.C. impose**: continuity of the total stress components, discontinuity of pressure proportional to averaged fluid velocities and discontinuities of displacements proportional to stress components and averaged fluid pressures.
- They allow to represent **wave-induced fluid flow (mesoscopic loss)** by which the fast waves are converted to slow (diffusive) Biot waves when travelling across fractures.

Boundary conditions at a fracture within a Biot medium. I

$\Omega = (0, L_1) \times (0, L_3)$ with boundary Γ in the (x_1, x_3) -plane,
 x_1, x_3 : horizontal and vertical coordinates, respectively.

Ω contains a set of horizontal fractures $\Gamma^{(f,l)}$, $l = 1, \dots, J^{(f)}$
each one of length L_1 and aperture $h^{(f)}$. This set of fractures
divides Ω in a collection of non-overlapping rectangles
 $R^{(l)}$, $l = 1, \dots, J^f + 1$.

Assume that the rectangles $R^{(l)}$ and $R^{(l+1)}$ have a fracture
 $\Gamma^{(f,l)}$ as a common side.

$[\mathbf{u}^s]$, $[\mathbf{u}^f]$: jumps of the solid and fluid displacement vectors
at $\Gamma^{(f,l)}$.

$\nu_{l,l+1}$ and $\chi_{l,l+1}$: the unit outer normal and a unit tangent
(oriented counterclockwise) on $\Gamma^{(f,l)}$ from $R^{(l)}$ to $R^{(l+1)}$.

Juan E. Santos,

Introduction

A viscoelastic
medium long-wave
equivalent to a
Biots medium. I

Variational
formulation. The
FEM

Application to the
cases of patchy
gas-brine
saturation and
highly
heterogeneous
frames

Fractured Biot
media

A VTI long-wave
equivalent to a
fractured Biots
medium. I

The Macroscale.
Wave propagation

$$[\mathbf{u}^s \cdot \nu_{l,l+1}] = \eta_N \left((1 - \alpha^{(f)}) \tilde{B}^{(f)} (1 - \Pi) \tau(\mathbf{u}) \nu_{l,l+1} \cdot \nu_{l,l+1} - \alpha^{(f)} \frac{1}{2} \left((-p_f^{(l+1)}) + (-p_f^{(l)}) \right) \Pi \right),$$

$$[\mathbf{u}^s \cdot \chi_{l,l+1}] = \eta_T \tau(\mathbf{u}) \nu_{l,l+1} \cdot \chi_{l,l+1},$$

$$[\mathbf{u}^f \cdot \nu_{l,l+1}] = \alpha^{(f)} \eta_N \left(-\tau(\mathbf{u}) \nu_{l,l+1} \cdot \nu_{l,l+1} + \frac{1}{\tilde{B}^{(f)}} \frac{1}{2} \left((-p_f^{(l+1)}) + (-p_f^{(l)}) \right) \right) \Pi,$$

$$(-p_f^{(l+1)}) - (-p_f^{(l)}) = \frac{i\mu^{(f)}}{\hat{\kappa}^{(f)}} \frac{1}{2} \left(\mathbf{u}_f^{(l+1)} + \mathbf{u}_f^{(l)} \right) \cdot \nu_{l,l+1},$$

$$\tau(\mathbf{u}) \nu_{l,l+1} \cdot \nu_{l,l+1} = \tau(\mathbf{u}) \nu_{l+1,l} \cdot \nu_{l+1,l},$$

$$\tau(\mathbf{u}) \nu_{l,l+1} \cdot \chi_{l,l+1} = \tau(\mathbf{u}) \nu_{l+1,l} \cdot \chi_{l+1,l},$$

η_N and η_T : normal and tangential fracture compliances.

Fracture dry plane wave and shear modulus

$H_m^{(f)} = K_m^{(f)} + \frac{4}{3}G^{(f)}$ and $G^{(f)}$ in terms of η_N, η_T :

$$\eta_N = \frac{h^{(f)}}{H_m^{(f)}}, \quad \eta_T = \frac{h^{(f)}}{G^{(f)}}.$$

$$\alpha^{(f)} = 1 - \frac{K_m^{(f)}}{K_s^{(f)}}, \quad \hat{\kappa}^{(f)} = \frac{\kappa^{(f)}}{h^{(f)}},$$

$$\epsilon = \frac{(1+i)}{2} \left(\frac{\eta^{(f)} \alpha^{(f)} \eta_N}{2 \tilde{B}^{(f)} \hat{\kappa}^{(f)}} \right)^{1/2}, \quad \Pi(\epsilon) = \frac{\tanh \epsilon}{\epsilon},$$

$$\tilde{B}^{(f)} = \frac{\alpha^{(f)} M^{(f)}}{H_u^{(f)}}, \quad H_u^{(f)} = K_u^{(f)} + \frac{4}{3}G^{(f)}.$$

A TIV medium equivalent to a Biot's medium with aligned fractures. I

- A Biot medium with a dense set of horizontal fractures behaves as a **Transversely Isotropic and Viscoelastic (TIV) medium** when the average fracture distance is much smaller than the predominant wavelength of the travelling waves.
- This leads to frequency and angular variations of velocity and attenuation of seismic waves.
- The time-harmonic experiments described before are generalized and applied to determine the **TIV medium long-wave equivalent** to a densely fractured Biot medium.

A TIV medium equivalent to a Biot's medium with aligned fractures. II

$\tilde{\sigma}_{ij}(\tilde{\mathbf{u}}^s)$, $e_{ij}(\tilde{\mathbf{u}}^s)$: stress and strain tensor components of the equivalent TIV medium

$\tilde{\mathbf{u}}^s$: solid displacement vector at the macro-scale.

The TIV stress-strain relations:

$$\tilde{\sigma}_{11}(\tilde{\mathbf{u}}^s) = p_{11} e_{11}(\tilde{\mathbf{u}}^s) + p_{12} e_{22}(\tilde{\mathbf{u}}^s) + p_{13} e_{33}(\tilde{\mathbf{u}}^s),$$

$$\tilde{\sigma}_{22}(\tilde{\mathbf{u}}^s) = p_{12} e_{11}(\tilde{\mathbf{u}}^s) + p_{11} e_{22}(\tilde{\mathbf{u}}^s) + p_{13} e_{33}(\tilde{\mathbf{u}}^s),$$

$$\tilde{\sigma}_{33}(\tilde{\mathbf{u}}^s) = p_{13} e_{11}(\tilde{\mathbf{u}}^s) + p_{13} e_{22}(\tilde{\mathbf{u}}^s) + p_{33} e_{33}(\tilde{\mathbf{u}}^s),$$

$$\tilde{\sigma}_{23}(\tilde{\mathbf{u}}^s) = 2 p_{55} e_{23}(\tilde{\mathbf{u}}^s),$$

$$\tilde{\sigma}_{13}(\tilde{\mathbf{u}}^s) = 2 p_{55} e_{13}(\tilde{\mathbf{u}}^s),$$

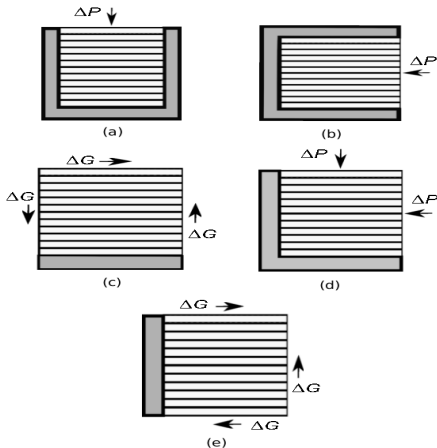
$$\tilde{\sigma}_{12}(\tilde{\mathbf{u}}^s) = 2 p_{66} e_{12}(\tilde{\mathbf{u}}^s).$$

$$p_{22} = p_{11}, \quad p_{23} = p_{13}, \quad p_{55} = p_{44}, \quad p_{12} = p_{11} - 2p_{66}.$$

A TIV medium equivalent to a Biot's medium with aligned fractures. III

- In the context of **Numerical Rock Physics** the complex stiffness coefficients $p_{IJ}(\omega)$ are determined using five time-harmonic experiments, each one associated with a BVP.
- The BVP's consist on **compressibility and shear tests** on a sample of Biot material with a dense set of fractures modeled using **B. C.**
- The BVP's are formulated in the space-frequency domain and solved using th FEM.
- This approach offers an alternative to laboratory measurements. It is essentially free from experimental errors and can easily be run using alternative models of the materials being analyzed.

The Experiments to Determine the Five p_{IJ} TIV Stiffness



(I) : Figures (a) and (b) show how to determine p_{33} and p_{11} ,
(c) determines p_{55} , (e) determines p_{66} and (d) determines
 p_{13} .

The procedure to determine the complex stiffnesses $p_{IJ}(\omega)$ at the macro-scale was validated by comparison with the analytical solution given by Krzikalla and Müller (GPY, 2011).

Next were applied to patchy brine-gas saturation, a case for which no analytical solutions are available.

Instead of the stiffnesses $p_{IJ}(\omega)$ the Figures display the the corresponding energy velocities and dissipation coefficients.

In all the experiments we used square samples of side length 2 m, with 9 fractures at equal distance of 20 cm and fracture aperture 1 mm.

The numerical samples were discretized with a 100×100 uniform mesh.

Table: Material properties of background and fractures

Background	Solid grains bulk modulus, K_s	36. GPa
	solid grains density, ρ_s	2700 kg/m ³
	Dry bulk modulus K_m	9 GPa
	shear modulus G	7 GPa
	Porosity ϕ	0.15
	permeability κ	0.1 Darcy
Fractures	Solid grains bulk modulus, K_s	36. GPa
	solid grains density, ρ_s	2700 kg/m ³
	Dry bulk modulus K_m	0.0055 GPa
	shear modulus G	0.0033 GPa
	Porosity ϕ	0.5
	permeability κ	10 Darcy

The properties of the saturant fluids, brine and gas, are the same than in the previous example for patchy saturation.

qP and qSV energy velocity at 30 Hz for full brine, full gas, 10% and 50% patchy gas-brine saturation.

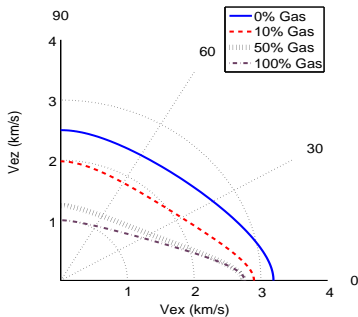


Figure 33 (a) : qP energy velocity
qP and qSV velocity decreases as gas saturation increases.

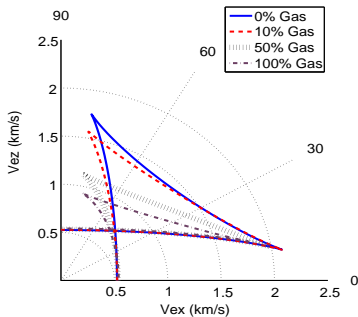
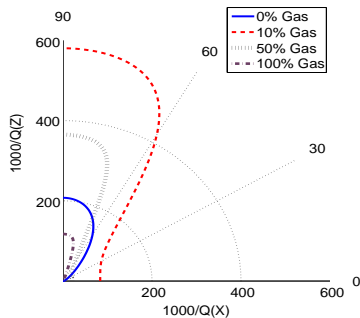


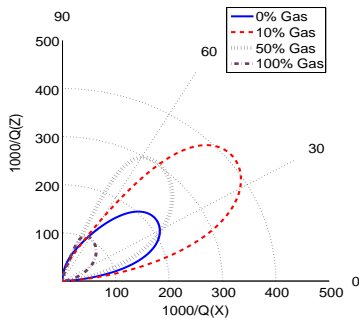
Figure 33 (b) : qSV energy velocity.
qSV velocity exhibits the typical cuspidal triangles.

qP and qSV dissipation factors at 30 Hz for full brine, full gas, 10% and 50% patchy gas-brine saturation.



(a)

Figure 34(a) : $\frac{1000}{qP}$



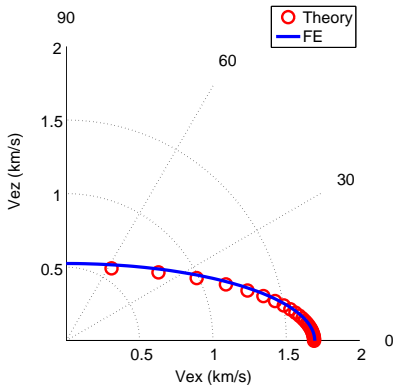
(b)

Figure 34 (b) : $\frac{1000}{qSV}$

qP anisotropy is enhanced by patchy saturation, is highest at 10 % gas saturation and with maximums for waves arriving normally to the fracture layering. qSV waves show maximum attenuation at 10 % gas saturation, with different anisotropic behaviour depending on gas saturation.

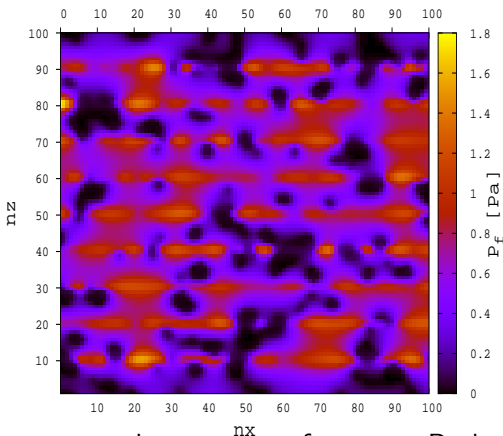
SH energy velocity at 30 Hz for full brine saturation. The SH polarization is normal to the plane (x_1, x_3)

that is the plane of the figure



SH waves show velocity anisotropy and they are lossless

Fluid pressure for normal compression to the fracture plane at 30 Hz and 10 % patchy gas saturation.



Higher pressure values occur at fractures. Darker regions identify gas patches. High pressure gradients at boundaries of fractures and patches show the mesoscopic loss effect.

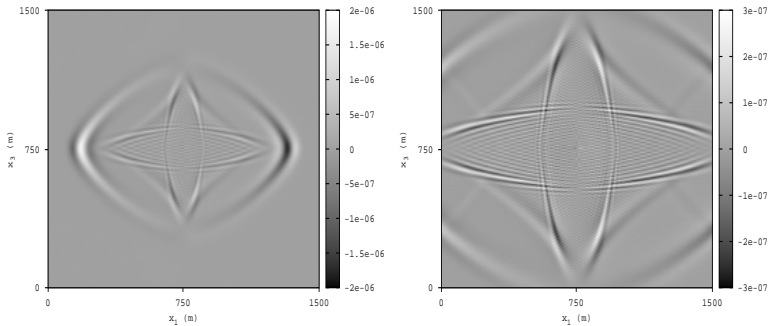
The Macroscale. Numerical modeling of wave propagation in a 3D VTI homogeneous medium equivalent to a densely fractured Biot medium

Consider a square computational domain of side length 1500 m and a compressional point source principal frequency 30 Hz located at the center of the domain.

The computational mesh is $200 \times 200 \times 200$, so that the mesh size is $h = 7.5$ m.

To model wave propagation in a densely fractured Biot medium we use a long-wave equivalent VTI medium with the p_{IJ} computed as explained above using the Numerical Rock Physics approach.

The solution of the equations of motion for the VTI medium was computed using a parallel implementation of a finite element domain decomposition procedure based on a nonconforming 3D FE space.



(a)

(b)

Figure 38 (a) : 200 ms

Figure 38 b) 300 ms

The faster wave front correspond to the qP wave, that moves faster in the horizontal than in the vertical direction, in accordance with the velocity graphs in Figure 33 a). The qSV wave shows vertical and horizontal wavefronts as well as the typical cusps (energy triPLICATION) in the triangular wavefronts at 45 degrees, as indicated in Figure 33 b).

At 300 ms the qP wavefront in Figure 38 b) is already leaving the computational domain, while the qSV wavefronts are arriving to the artificial boundaries. Note that the absorbing boundary conditions for TIV media are working quite well, no spurious reflections from the artificial boundaries are observed.

Juan E. Santos,

Introduction

A viscoelastic
medium long-wave
equivalent to a
Biot's medium. I

Variational
formulation. The
FEM

Application to the
cases of patchy
gas-brine
saturation and
highly
heterogeneous
frames

Fractured Biot
media

A VTI long-wave
equivalent to a
fractured Biot's
medium. I

The Macroscale.
Wave propagation

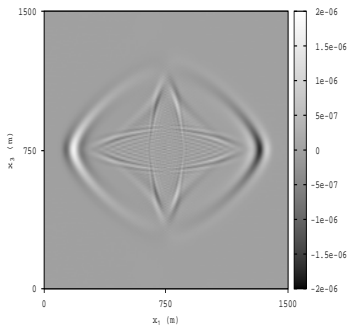


Figure 39 (a)

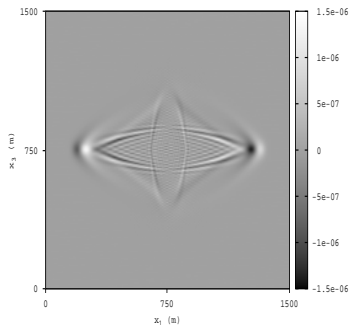


Figure 39 (b)

Figure 39 (a) : Brine saturation in background and fractures, Figure 39 (b) : Patchy gas-brine saturation in background and fractures with 10% overall gas saturation
The fast wave front in Figure 39 a) corresponds to the qP wave, that it is not seen in 39 b) because of the high attenuation of this wave in direction normal to the fracture layering (see Figure 34 a). qSV wavefronts in Figure 39 b) move slowly and more attenuated than in Figure 39 a), in accordance with the velocity and attenuation graphs in Figures 33 b) and 34 b)

Snapshots of x -component of VTI displacements at 200 ms in (x, z) -plane. Full brine versus 50% patchy

gas-brine saturation.

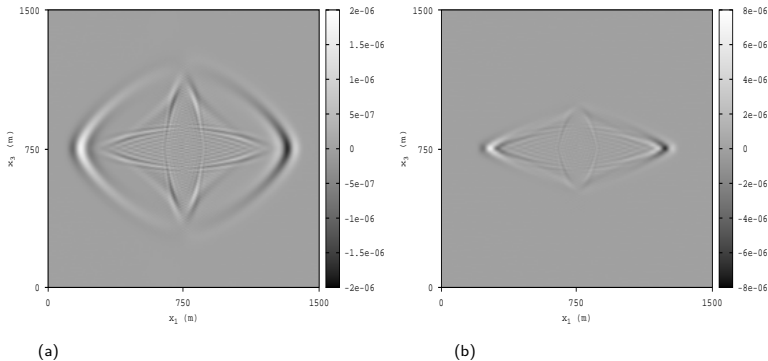


Figure 40 (a) : Full brine saturation, Figure 40 (b) : Patchy gas-brine saturation in background and fractures with 50% overall gas saturation. qSV wavefronts in Figure 40 b) are not as well defined as in the case of 10% patchy gas-brine saturation in 39 b). The triangular cusps are still present close to the vertical direction but not as well defined as in Figure 40 a).

The macro-scale. Seismic monitoring of CO₂ sequestration. I

- Capture and storage of carbon dioxide in deep saline aquifers and aging oil reservoirs is a valid alternative approach for reducing the amount of greenhouse gases in the atmosphere
- We model CO₂ injection in the Utsira formation at the Sleipner gas field in the North Sea.
- Within the formation, there are several mudstone layers acting as barriers to the vertical flow of CO₂. Injection started in 1996 at a rate of about one million tonnes per year.
- A petrophysical model of the Utsira formation is built based on fractal porosity and clay content, taking into account the variation of properties with pore pressure and saturation.

The macro-scale. Seismic monitoring of CO₂ sequestration. II

- We describe a methodology to model the CO₂ flow and monitor the storage combining numerical simulations of CO₂-brine flow and seismic wave propagation.
- Flow of brine and CO₂ is modeled with the Black-Oil formulation for two-phase flow in porous media.
- A space-frequency domain wave propagation simulator is used to monitor the injection. A Zener model is used to determine the P and S waves moduli in the brine saturated zones.
- In zones where CO₂ is present, patchy CO₂-brine distribution is assumed and the time-harmonic compressibility tests are used to model P-wave velocity and attenuation. The S modulus is determined using a mechanism related to the P-modulus.

The pressure dependence of properties is based on the following relationship between porosity and pore pressure

$$p(t) = S_b p_b(t) + S_g p_g(t):$$

$$\frac{(1 - \phi_c)}{K_s} (p(t) - p_H) = \phi_0 - \phi(t) + \phi_c \ln \frac{\phi(t)}{\phi_0}$$

S_b, S_g : brine and CO_2 saturations, ϕ_c : a critical porosity
 $\phi_0 = \phi_0(x, z)$: initial porosity at hydrostatic pore pressure
 p_H , assumed to have a fractal spatial distribution around the average porosity $\langle \phi_0 \rangle$, obtained from the neutron log.
 K_s : bulk modulus of the solid grains, computed as the arithmetic average of the Hashin Shtrikman upper and lower bounds of quartz (bulk modulus of 40 GPa) and clay (bulk modulus of 15 GPa).

Relationship among horizontal permeability (κ_{x_1}), porosity and clay content (C):

$$\frac{1}{\kappa_{x_1}(t)} = \frac{45(1 - \phi(t))^2}{\phi(t)^3} \left(\frac{(1 - C)^2}{R_q^2} + \frac{C^2}{R_c^2} \right),$$

R_q, R_c : average radii of the sand and clay grains, respectively.
Assumed relation between the horizontal and vertical permeabilities $\kappa_{x_1}, \kappa_{x_3}$:

$$\frac{\kappa_{x_1}(t)}{\kappa_{x_3}(t)} = \frac{1 - (1 - 0.3a)\sin(\pi S_b)}{a(1 - 0.5\sin(\pi S_b))},$$

a : permeability-anisotropy parameter ($a= 0.1$ here)).

The bulk and shear moduli of the dry matrix, K_m, μ_m are computed using the Krief model:

$$K_m(t) = K_s(1 - \phi(t))^{A/(1-\phi(t))},$$

$$\mu_m(t) = \mu_s(1 - \phi(t))^{A/(1-\phi(t))}$$

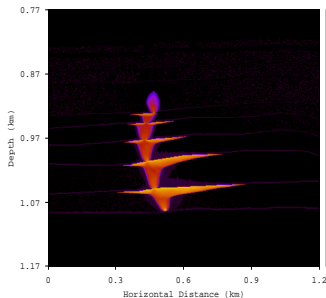
Using the moduli K_S, μ_S, K_m, μ_m , porosity ϕ and permeabilities κ_X, κ_Z , the fluids bulk moduli and viscosities and the CO₂ saturation map we determine the complex and frequency dependent P-wave and S moduli at each computational cell using the harmonic experiments. The flow simulator model uses the following relative permeabilities and capillary pressure functions:

$$K_{rg}(S_g) = K_{rg}^* \left(\frac{S_g - S_{gc}}{1 - S_{gc} - S_{bc}} \right)^{n_g}$$

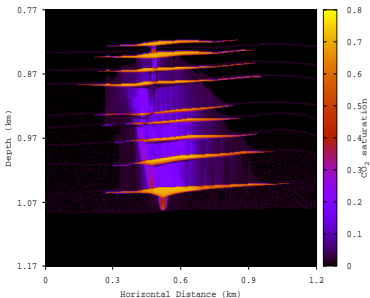
$$K_{rb}(S_g) = K_{rb}^* \left(\frac{1 - S_g - S_{bc}}{1 - S_{gc} - S_{bc}} \right)^{n_b},$$

$$P_{ca}(S_g) = P_{ca}^* \left(\frac{S_g - S_{gc}}{1 - S_{gc} - S_{bc}} \right)^{n_c}.$$

S_{gc} and S_{bc} : saturations at which the CO₂ and brine phases become mobile.

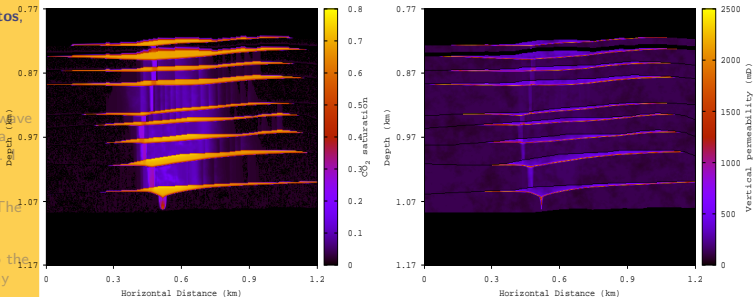


(a) CO₂ saturation after 1 year of injection



(b) CO₂ saturation after 3 years of injection

CO₂ is seen to move upwards and accumulate below the mudstone layers.



(a) CO₂ saturation after 7 years of injection

(b) Vertical permeability after seven years of CO₂ injection.

In Figure a) CO₂ continues to move upwards and accumulate below the mudstone layers. Figure b) shows the updated saturation dependent vertical permeability.

Time-lapse seismics applied to monitor CO₂ sequestration. I

- We use 2-D slices of CO₂ saturation and fluid pressure maps obtained from the flow simulator to construct a 2-D model of the Utsira formation. The mesh is 600 cells in the x_1 -direction and 200 cells in the x_3 -direction.
- The seismic source is a spatially localized plane wave of main frequency 60 Hz located at $z = 772$ m. A line of receivers is located at the same depth to record the Fourier transforms of the vertical displacements.
- The plane-wave simulation (a flat line of point sources at each grid point at the surface) is a good approximation to the stack.

Juan E. Santos,

Introduction

A viscoelastic
medium long-wave
equivalent to a
Biots medium. I

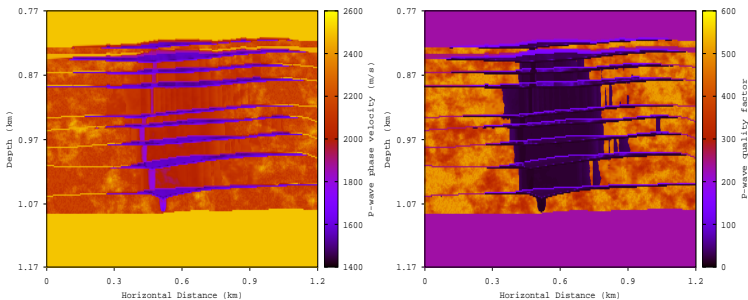
Variational
formulation. The
FEM

Application to the
cases of patchy
gas-brine
saturation and
highly
heterogeneous
frames

Fractured Biot
media

A VTI long-wave
equivalent to a
fractured Biots
medium. I

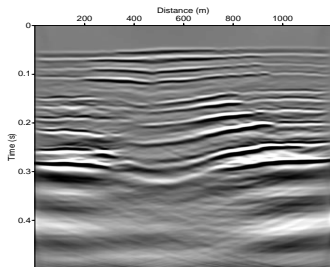
The Macroscale.
Wave propagation



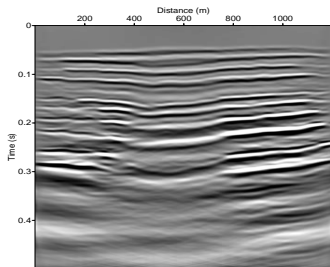
(a) v_p map at 50 Hz after 7 years of CO₂ injection

(b) Q_p map at 50 Hz after 7 years of CO₂ injection

This Figures show how the injected CO₂ change P-wave velocities and quality factors v_p and Q_p ; both decrease in the CO₂-saturated zones. A lower value of Q_p indicates a higher attenuation.

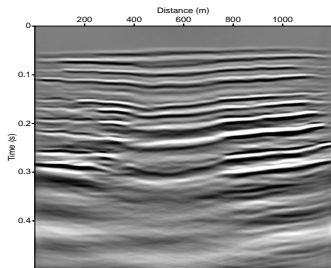


(a) Seismogram after 3 years of CO₂ injection.

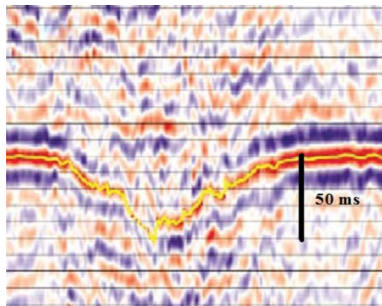


(b) Seismogram after 7 years of CO₂ injection.

Figures a) and b) show how CO₂ moves upwards and accumulates below the mudstone layers. the pushdown effect is clearly observed



(a) Seismogram after 3 years of CO₂ injection.



(b) Seismogram after 7 years of CO₂ injection.

Figures a) and b) show the delay in the arrival times of the reflections, the pushdown effect and the strong attenuation in the chimney region observed in real seismograms. The delay has been properly matched in the simulations.

THANKS FOR YOUR ATTENTION

!!!!

A Numerical
Rocks Physics
Approach to
Model Wave
Propagation in
Hydrocarbon
Reservoirs

Juan E. Santos,

Introduction

A viscoelastic
medium long-wave
equivalent to a
Biot's medium. I

Variational
formulation. The
FEM

Application to the
cases of patchy
gas-brine
saturation and
highly
heterogeneous
frames

Fractured Biot
media

A VTI long-wave
equivalent to a
fractured Biot's
medium. I

The Macroscale.
Wave propagation